

Supporting Information

In-MOF-Derived Ultrathin Heteroatom-Doped Carbon Nanosheets for Improving Oxygen Reduction

Qi Huang^{a,b}, Yuanyuan Guo^a, Xian Wang^a, Lulu Chai^a, Junyang Ding^a, Li Zhong^a,
Ting-Ting Li^c, Yue Hu^{a,*}, Jinjie Qian^{a,b,*}, Shaoming Huang^{d,*}

Dedicated to the 60 years of the Fujian Institute of Research on the Structure of Matter

^a *Key Laboratory of Carbon Materials of Zhejiang Province, College of Chemistry and Materials Engineering, Wenzhou University, Wenzhou, 325000, China*

^b *State Key Laboratory of Structural Chemistry, Fujian Institute of Research on the Structure of Matter, Chinese Academy of Sciences, Fuzhou, 350002, China*

^c *Chemistry Institute for Synthesis and Green Application, School of Materials Science and Chemical Engineering, Ningbo University, Ningbo, 315211, China*

^d *School of Materials and Energy, Guangdong University of Technology, Guangzhou, Guangdong 510006, China*

Experimental Section

Materials

The following materials are used without further purification as receiving materials. Indium nitrate hydrate ($\text{In}(\text{NO}_3)_3 \cdot x\text{H}_2\text{O}$, 99.9%, Aladdin), Iron(III) chloride (FeCl_3 , AR, Aladdin), Cobalt chloride hexahydrate ($\text{CoCl}_2 \cdot 6\text{H}_2\text{O}$, AR, Aladdin), 4,5-Imidazoledicarboxylic acid (H_3ImDC , 97%, Aladdin), Ammonium thiocyanate (NH_4SCN , AR, Aladdin), NH_4Cl (AR, 99.5%, Aladdin), Activated carbon (Nanjing Xianfeng), Ammonia solution (25%–28%, AR, Aladdin), HCl (36–38%, AR, Jinshan Chemical), KOH (AR, 90%, Aladdin), JM 20 wt% Pt/C (HISPEC 3000), *N,N*-dimethylformamide (DMF, AR, 99.5%, Aladdin), Acetonitrile (MeCN, AR, 99%, Aladdin), Acetic acid (CH_3COOH , AR, 99.5%, Aladdin), Ethanol (AR, 95%, Aladdin), Nafion solution (5 wt %, Dupont) and distilled water. All experiments are performed with high-purity N_2 , O_2 and Ar gases of 99.999%.

Synthesis of InOF-24

$\text{In}(\text{NO}_3)_3 \cdot x\text{H}_2\text{O}$ (30 mg, 0.1 mmol) and H_3ImDC (30 mg, 0.2 mmol) are dissolved in a mixed solution of DMF/MeCN (3/3 mL). Acetic acid (50 μL) is then added as a pH regulator. The solution is placed in a 25 mL glass bottle in an oven at 85 °C for 4 days. The obtained crystals are washed with ethanol and soaked in ethanol solution for 12 h to replace guest molecules to obtain **InOF-24**.

Synthesis of $[\text{Fe}(\text{SCN})_6]^{3-}$

FeCl₃ (40 mg, 0.25 mmol) and NH₄SCN (57 mg, 0.75 mmol) are dissolved in water (50 mL) and stirred to form a solution of 5 mmol·L⁻¹ of [Fe(SCN)₆]³⁻ complex.

Synthesis of [Co(NH₃)₆]Cl₃

After the solution of CoCl₂·6H₂O (240 mg, 1 mmol) and NH₄Cl (160 mg, 3 mmol) are dissolved in water (2 mL), activated carbon (4 mg) and ammonia solution (500 mL) are added. Then the solution is left in the air for 4 hours until the red turned to brownish. The solution is filtered to obtain filter residue containing precipitated crystals and activated carbon. The filter residue is poured into 15 mL water containing 0.30 mL concentrated HCl. The mixture is heated and dissolved before filtration. Add 4ml concentrated HCl to filtrate and slowly cool down to obtain orange precipitation. The precipitation recrystallization is purified to obtain pure [Co(NH₃)₆]Cl₃ coordination complex.

Synthesis of InFe@CNS900

InOF-24 (50 mg) is poured into 5 mmol·L⁻¹ [Fe(SCN)₆]³⁻ complex solution (50 mL) and allowed to stand for 8 h. Then, the [Fe(SCN)₆]³⁻ complex on the surface of crystals is washed with ethanol and dried for 2 h in a vacuum drying oven to obtain Fe(SCN)₆@**InOF-24**. The compound is placed in a vacuum tube filled with argon gas (100 sccm), heated to 900 °C with the heating rate of 10 °C·min⁻¹, and maintained for 3 h to get **InFe@CNS900**.

Synthesis of InCo@CN900

InOF-24 (50 mg) and $\text{Co}(\text{NH}_3)_6\text{Cl}_3$ (10.7 mg, $0.8 \text{ mmol}\cdot\text{g}^{-1}$) are poured into water (50 ml) and allowed to stand for 8 h. Then, the **InCo@CN900** is produced in the same way as the **InFe@CNS900**.

Synthesis of InFeCo@CNS700-1000

InOF-24 (50 mg) and $\text{Co}(\text{NH}_3)_6\text{Cl}_3$ (10.7 mg, $0.8 \text{ mmol}\cdot\text{g}^{-1}$) are poured into $5 \text{ mmol}\cdot\text{L}^{-1}$ $[\text{Fe}(\text{SCN})_6]^{3-}$ solution (50 mL) and allowed to stand for 8 h. Then, the $\text{Co}(\text{NH}_3)_6\text{Cl}_3$ and $[\text{Fe}(\text{SCN})_6]^{3-}$ on the surface of the obtained crystals are washed with ethanol and dried for 2 h in a vacuum drying oven to obtain the multi-component material. The compound is placed in a vacuum tube filled with argon gas (100 scm), heated to 700, 800, 900 and 1000 °C with the heating rate of $10 \text{ }^\circ\text{C}\cdot\text{min}^{-1}$, and maintained for 3 h to get **InFeCo@CNS700**, **InFeCo@CNS800**, **InFeCo@CNS900**, and **InFeCo@CNS1000**, respectively.

Instrumentation and methods

The powder X-ray diffraction patterns (PXRD) are operated on a Bruker D8 Advance powder diffractometer operating at 40 kV, 40 mA for Cu $K\alpha$ radiation ($\lambda = 0.154 \text{ nm}$).

Gas adsorption measurements are measured in the Specific Surface Area & Pore Size Analyzer (BSD-PS1), where the samples are placed in a clean ultra-high vacuum system, and the N_2 sorption measurement is collected in the liquid nitrogen at 77 K.

The scanning electron microscopy (SEM) images are obtained with a JEOL JSM

6700F field emission scanning electron microscope. High-resolution transmission electron microscope (HRTEM) and energy dispersive X-ray spectroscopy (EDS) analyses are carried out under the JEOL JEM-2100F microscope with an acceleration voltage of 200 kV. The graphitization degree and defect of the samples are studied by Raman spectrometer with excitation from the 532 nm line. X-ray photoelectron spectroscopy (XPS) is conducted on a Thermo Scientific ESCALAB 250.

Electrochemical measurements

The as-synthesized catalyst (5 mg) is dispersed in ethanol (400 μL) and H_2O (100 μL), then the Nafion solution (5 wt%, 50 μL) is added under sonication for 1 h to form a homogeneous catalyst ink. Next, the 30 μL of the catalyst ink is pipetted onto the glassy carbon rotating ring disk electrode (RRDE, diameter 5.6 mm) used as the working electrode, in sequence and dry in the air, leading to a catalyst loading of 1.1 $\text{mg}\cdot\text{cm}^{-2}$.

The electrochemical measurements are conducted on an Autolab electrochemical workstation with a standard three-electrode system. The Ag/AgCl electrode and carbon rod are used as the reference and counter electrodes, respectively. All the electrochemical measurements are performed at room temperature and all potentials are presented relative to the reversible hydrogen electrode (RHE):

$$E_{RHE} = E_{Ag/AgCl} + 0.198 + 0.059 \times pH$$

Cyclic voltammetry (CV) measurements are carried out in N₂-/O₂-saturated 0.1 M KOH solution with a scan rate of 10 mV·s⁻¹. The linear sweep voltammogram (LSV) curves are performed in N₂-/O₂-saturated 0.1 M KOH solution at a rotation rate of 1600 rpm with the scan rate of 5 mV·s⁻¹ by RRDE. To evaluate the active surface area of catalysts, the double-layer capacitance (C_{dl}) is estimated by measuring the CV plots in the region from 1.00 to 1.10 V vs. RHE at various scan rates from 5 to 80 mV·s⁻¹ in 0.1 M N₂-saturated KOH. By fitting the current density at 1.05 V vs. RHE at various scan rates, the linear trend is observed and equal to the slope of the linear C_{dl}. The Koutecky-Levich (K-L) is analyzed at various electrode potentials. The electron transfer numbers (*n*) and the HO₂⁻ yields are calculated according to the K-L equations:

$$\frac{1}{J} = \frac{1}{J_L} + \frac{1}{J_K} = \frac{1}{B\omega^{1/2}} + \frac{1}{J_K}$$

$$J_L = 0.2nFC_0D_0^{2/3}\nu^{-1/6}\omega^{-1/2} = B\omega^{-1/2}$$

$$n = \frac{4I_d}{I_d + I_r/N}$$

$$HO_2^- (\%) = \frac{2I_r/N}{|I_d| + \frac{I_r}{N}} \times 100\%$$

In these formulas, *J*, *J_L*, and *J_K* is the experimental current density, diffusion-limited current density and kinetic current density, respectively; *ω* is the rotation speed in rpm (round per minute), *F* is the Faraday constant (96485 C·mol⁻¹), *C₀* is the bulk concentration of O₂ (1.2 × 10⁻⁶ mol·cm⁻³), *D₀* is the diffusion coefficient of O₂ in 0.1 M KOH (1.9 × 10⁻⁵ cm²·s⁻¹), and *ν* is the kinetic viscosity (0.01 cm²·s⁻¹). The *n* can be

extracted from the slope of the K-L plot. I_r is the ring current, I_d is the disk current and N expresses to the collection efficiency of the ring electrode (0.37). Stability test is taken by chronoamperometric measurement at a constant voltage of 0.615 V vs RHE in O₂-saturated 0.1 M KOH at a rotation rate of 1600 rpm.

A Nyquist plot is a parametric plot of a frequency response used in automatic control and signal processing which can be obtained by the EIS. The most common use of Nyquist plots is for assessing the stability of a system with feedback. And the detailed EIS dates are conducted by applying AC voltage at the 0.7 V vs. RHE with 10 mV amplitude in a frequency range from 10⁶ Hz to 0.1 Hz.

Zn-air battery assembly: the home-made Zn-air battery is assembled with a customized electrochemical cell, in which the electrocatalyst is conveniently coated on a carbon paper with a loading mass of 1.0 mg cm⁻² as cathode; a polished zinc plate is used as anode, and 6.0 M KOH is used as electrolyte. The obtained Zn-air battery is tested in ambient condition by Autolab electrochemical station.

Crystal data and refinement results

Table S1 Summary of Crystal Data and Refinement Results for **InOF-24**.

Items	InOF-24
CCDC	1978532
Formula	C ₆ H ₁ N ₂ O ₅ In _{0.5}
Mass	420.98
crystal system	cubic
space group	<i>Im-3m</i>
<i>a</i> (Å)	31.3413(7)
<i>b</i> (Å)	31.3413(7)
<i>c</i> (Å)	31.3413(7)
α (°)	90.00
β (°)	90.00
γ (°)	90.00
<i>V</i> (Å ³)	30786(2)
<i>T</i> (K)	295 (2)
<i>Z</i>	48
F(000)	9744
R _{int}	0.0686
R ₁ (I>2σ(I))	0.2160
wR ₂ (all reflections)	0.2453

Topological Analysis

4,5-imidazoledicarboxylate ligands can be regarded as 2-connected nodes in the obtained InOF-24, which can be ignored in the topological analysis. These In(III) centers are simplified as 4-connected nodes, the detailed calculation are listed below.

Topology for In1

Atom In1 links by bridge ligands and has

Common vertex with					R(A-A)	
In 1	0.1044	0.2500	0.3956	(0 0 0)	6.395A	1
In 1	0.2500	0.3956	0.1044	(0 0 0)	6.395A	1
In 1	-0.1044	0.3956	0.2500	(0 0 0)	6.487A	1
In 1	0.1044	0.6044	0.2500	(0 1 0)	6.487A	1

Structure consists of 3D framework with In

Coordination sequences

In1: 1 2 3 4 5 6 7 8 9 10

Num 4 9 17 28 42 60 81 105 132 162

Cum 5 14 31 59 101 161 242 347 479 641

TD10=641

Vertex symbols for selected sublattice

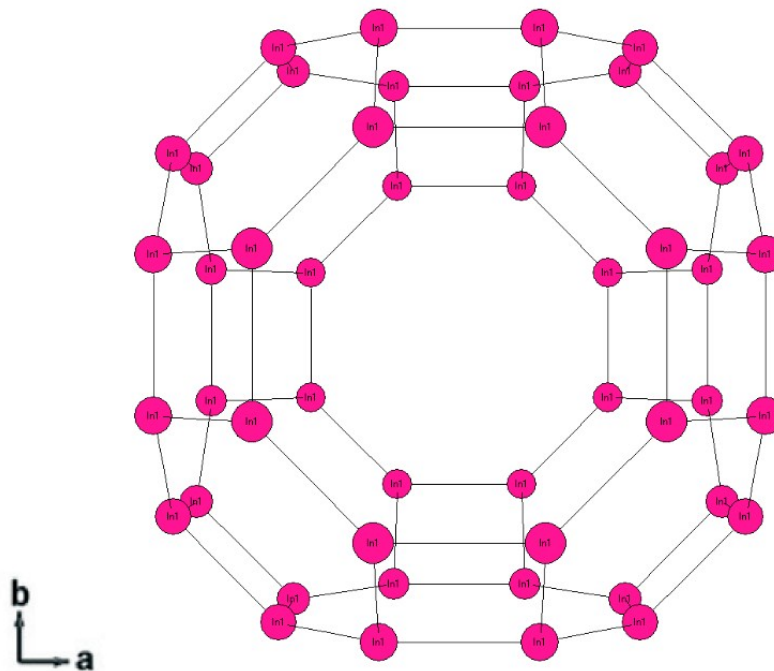
In1 Point (Schlafli) symbol:{4³.6³}

Extended point symbol:[4.4.4.6.6.6]

Point (Schlafli) symbol for net: {4³.6³}

4-c net; uninodal net

Topological type: rho/RHO; 4/4/c4; sqc11215 (topos&RCSR.ttd) {4³.6³} - VS
[4.4.4.6.8.8] (71251 types in 10 databases)



Characterization

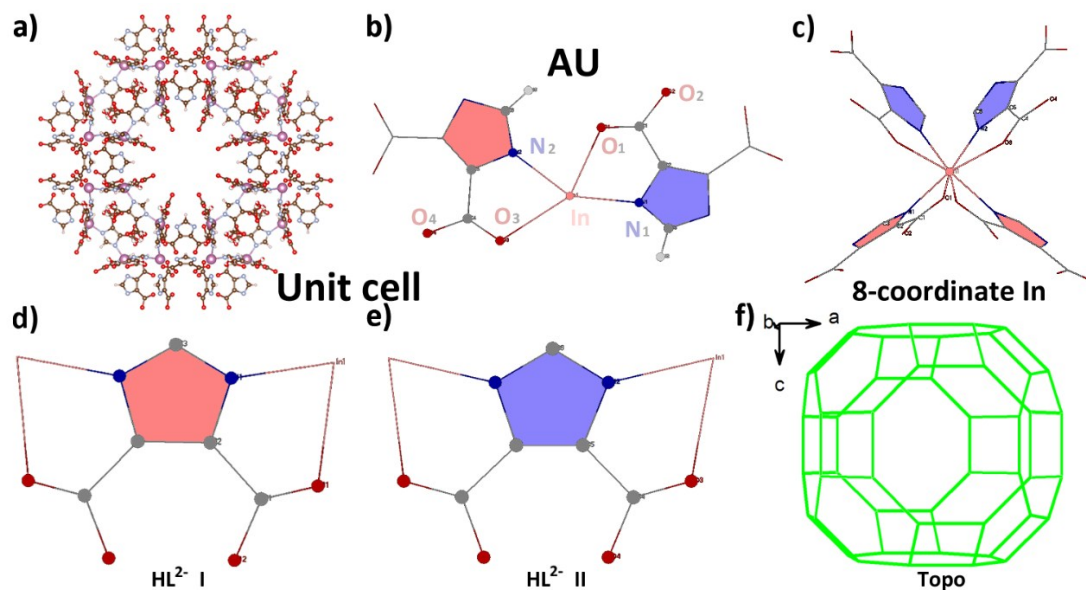


Figure S1. (a) Unit cell of **InOF-24**, (b) the asymmetric unit, (c) the 8-coordinate In cation, (d) the 2-connected HL²⁻ I, (e) the 2-connected HL²⁻ II, (f) its topological cell.

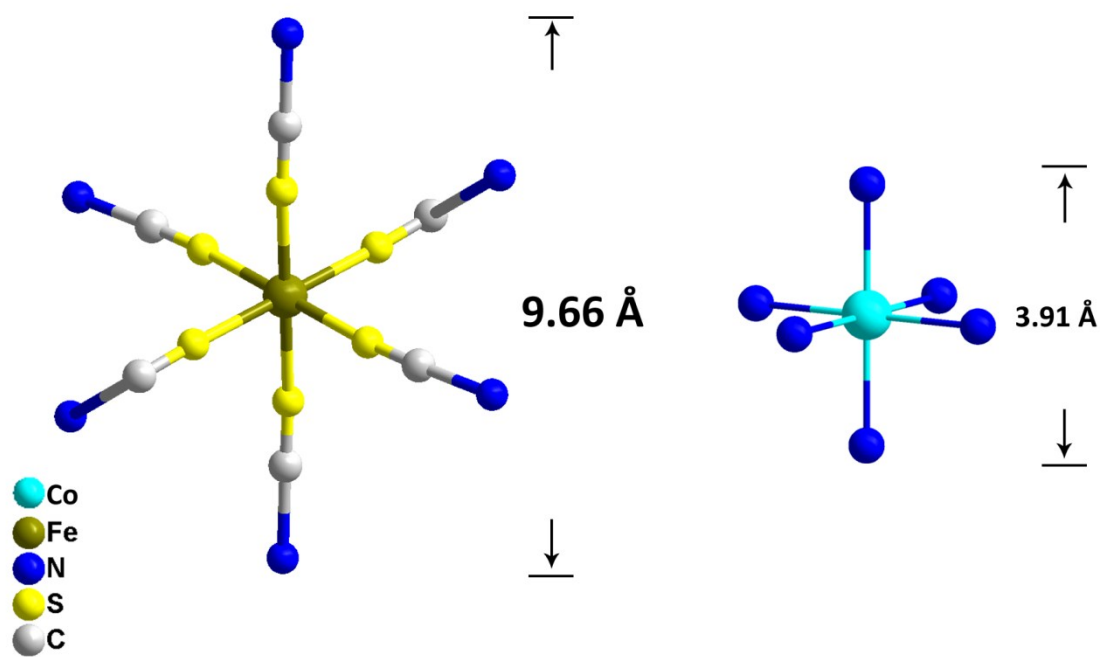


Figure S2. The molecular sizes of $[\text{Fe}(\text{SCN})_6]^{3-}$ (Left) and $[\text{Co}(\text{NH}_3)_6]^{3+}$ (Right) coordination complexes.

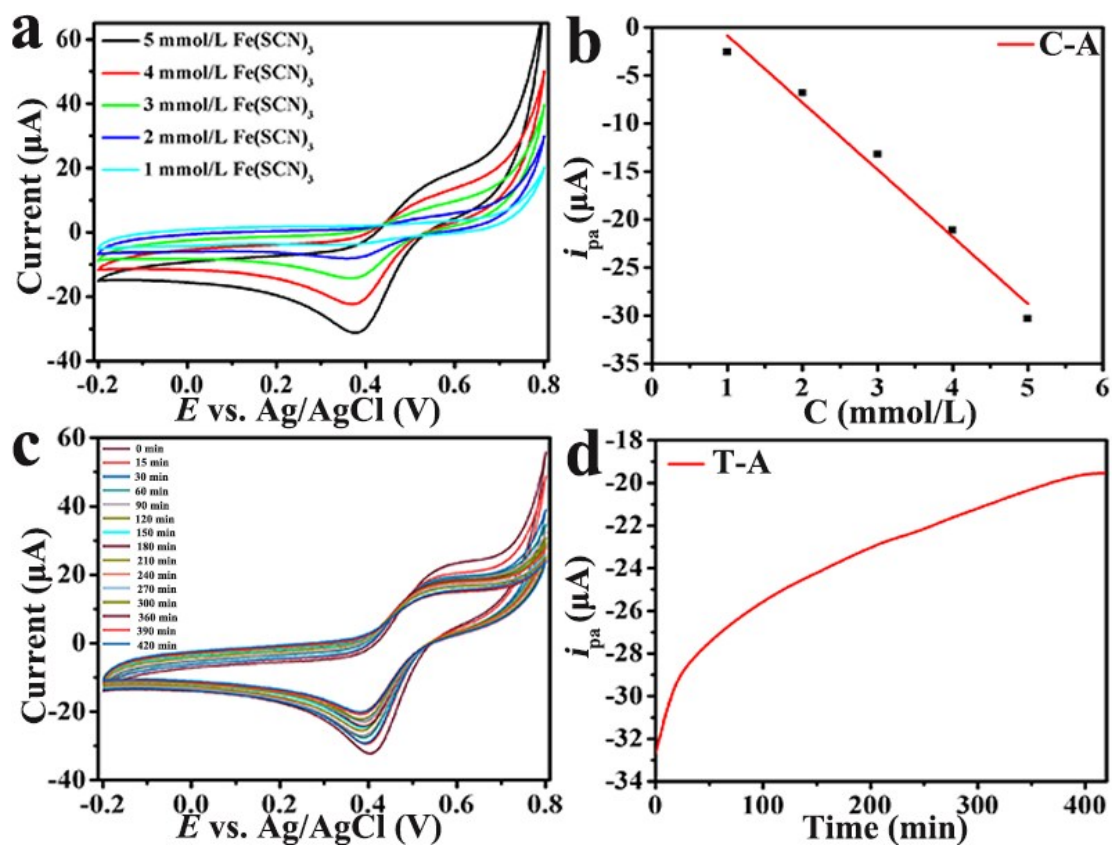


Figure S3. (a) CV curves of $[\text{Fe}(\text{SCN})_6]^{3-}$ complex solutions at different concentrations, (b) the linear relationship between the concentration of $[\text{Fe}(\text{SCN})_6]^{3-}$ complex solution and the reduction current, (c) CV curves of absorption of $[\text{Fe}(\text{SCN})_6]^{3-}$ in 5 mmol $\cdot\text{L}^{-1}$ $[\text{Fe}(\text{SCN})_6]^{3-}$ complex solution and (d) a diagram of the time and absorption of $[\text{Fe}(\text{SCN})_6]^{3-}$ in 5 mmol $\cdot\text{L}^{-1}$ $[\text{Fe}(\text{SCN})_6]^{3-}$ complex solution.

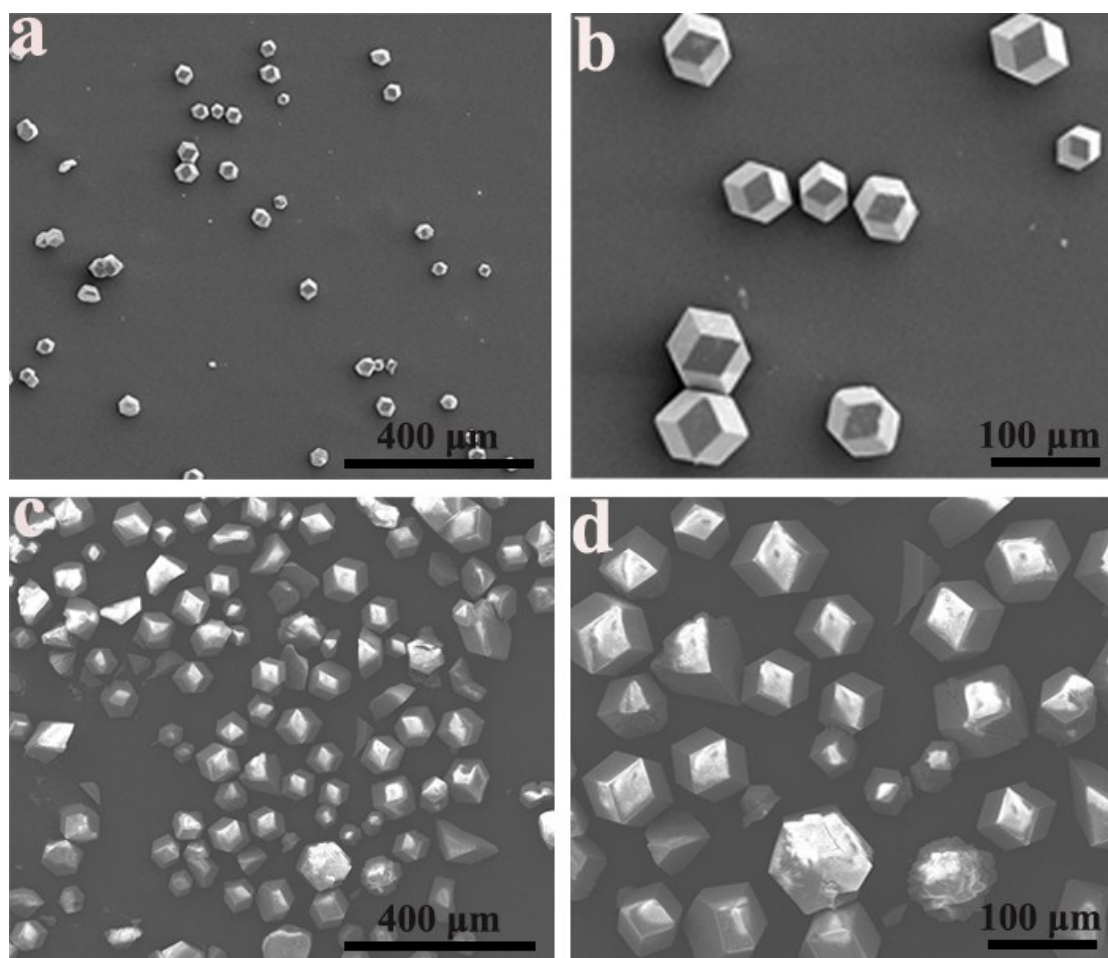


Figure S4. SEM images of (a, b) **InOF-24** and (c, d) **Fe(SCN)₆@InOF-24**.

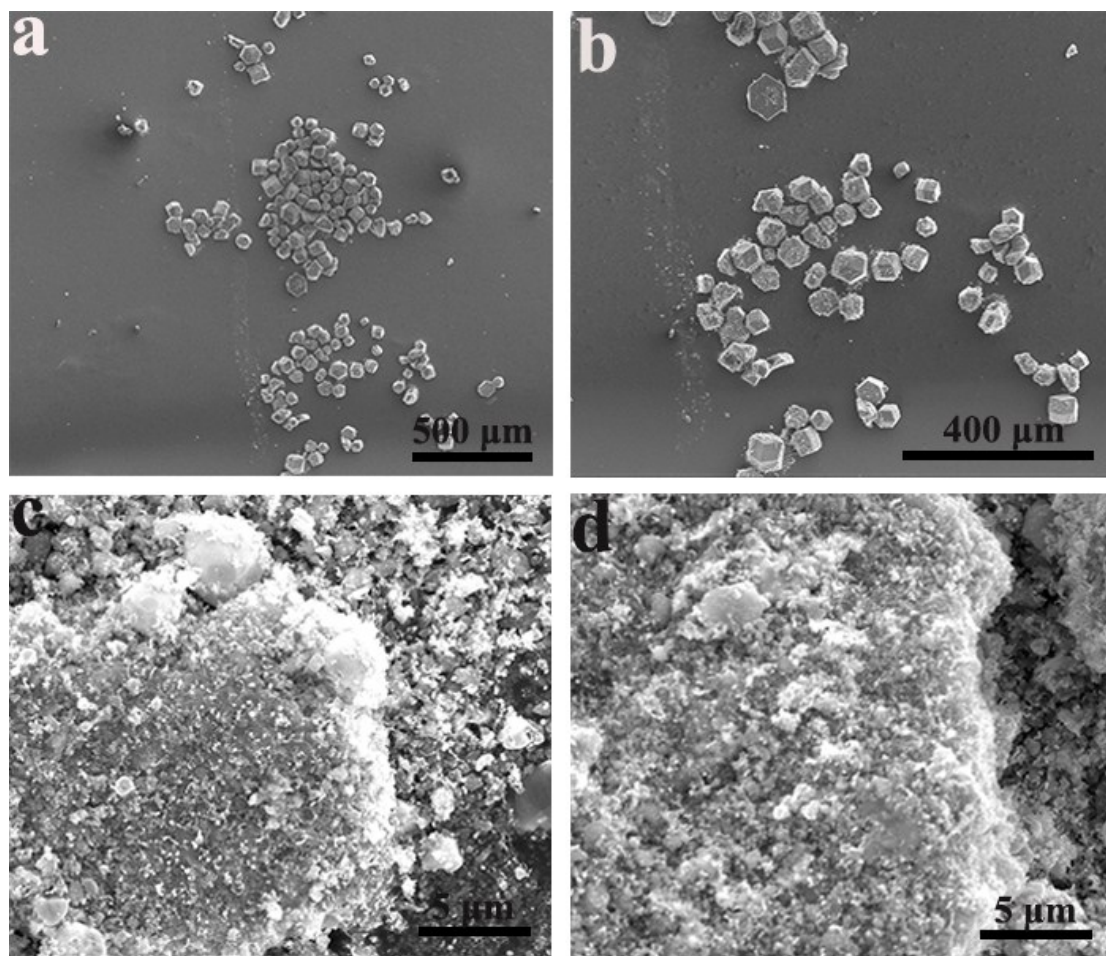


Figure S5. SEM images of (a, b) **InFe@CNS900** and (c, d) **InCo@CN900**.

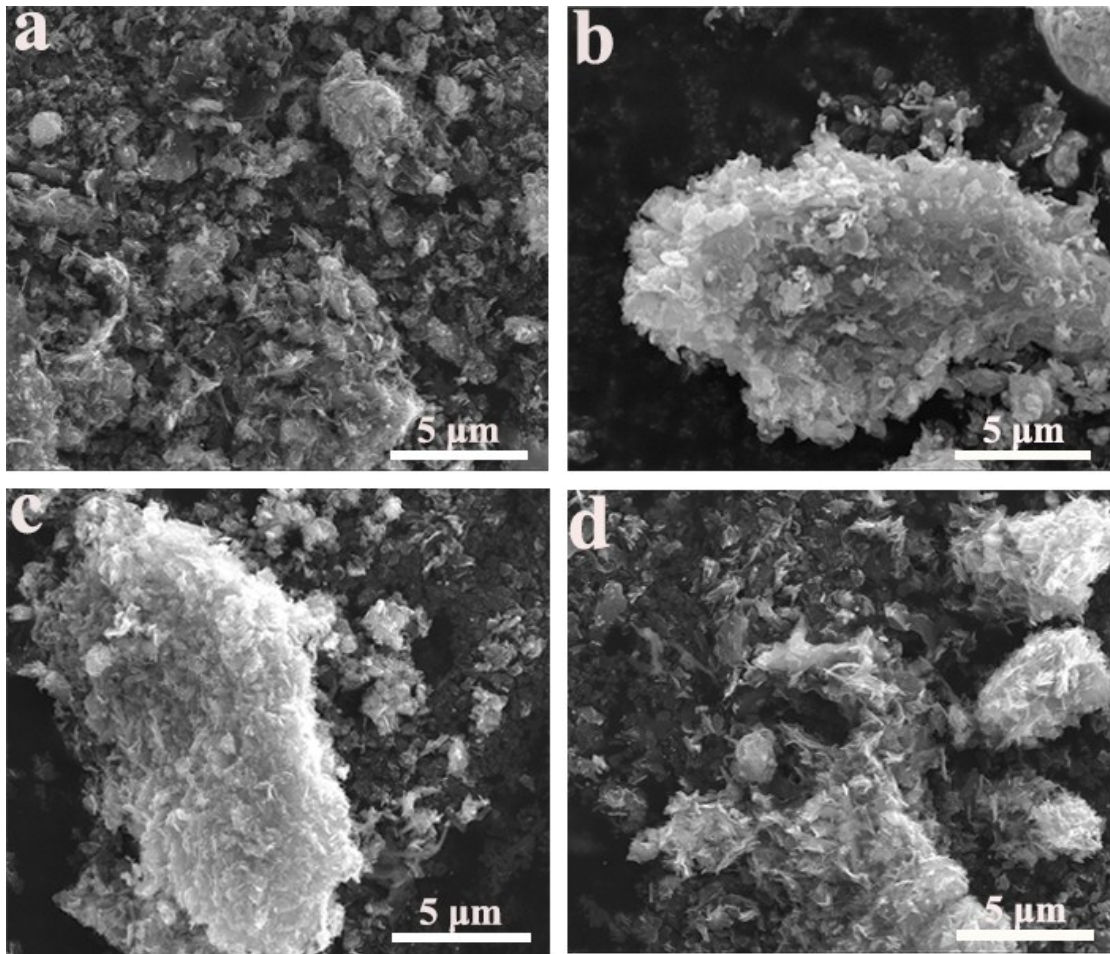


Figure S6. SEM images of **InFeCo@CNS900**.

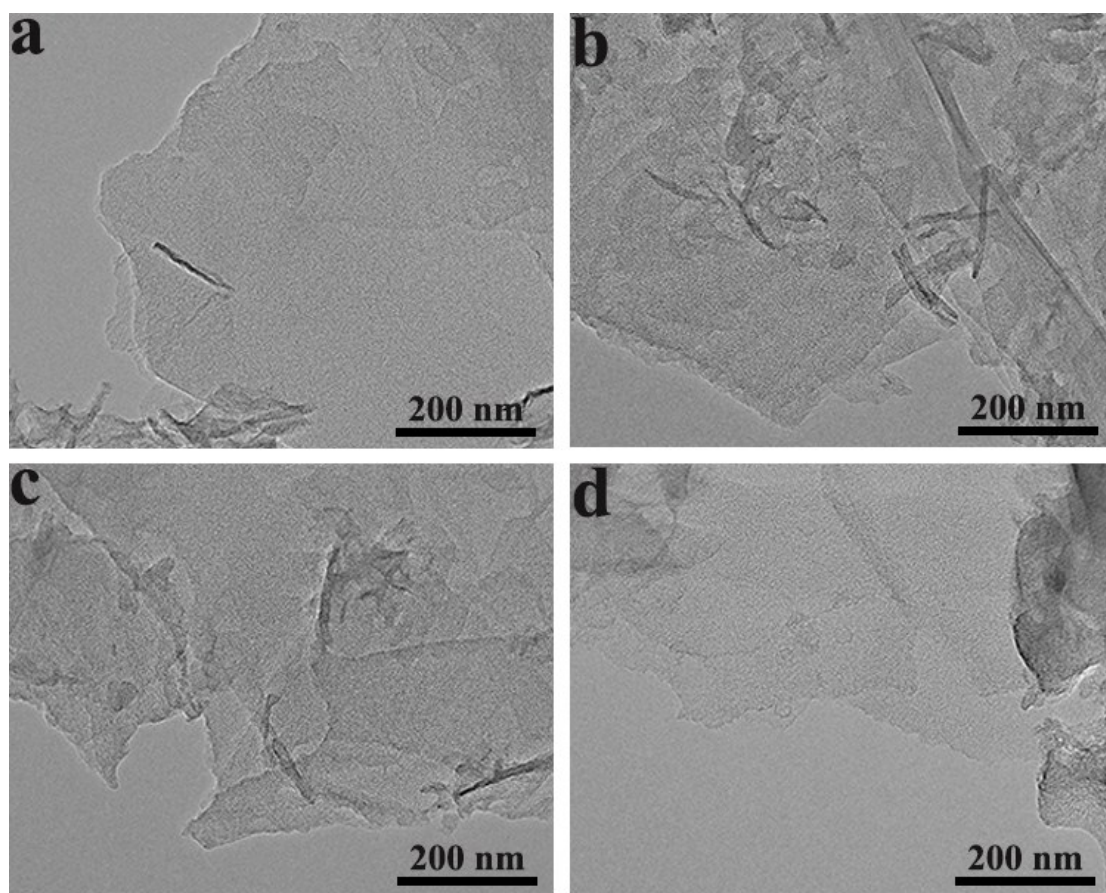


Figure S7. TEM images of InFeCo@CNS900.

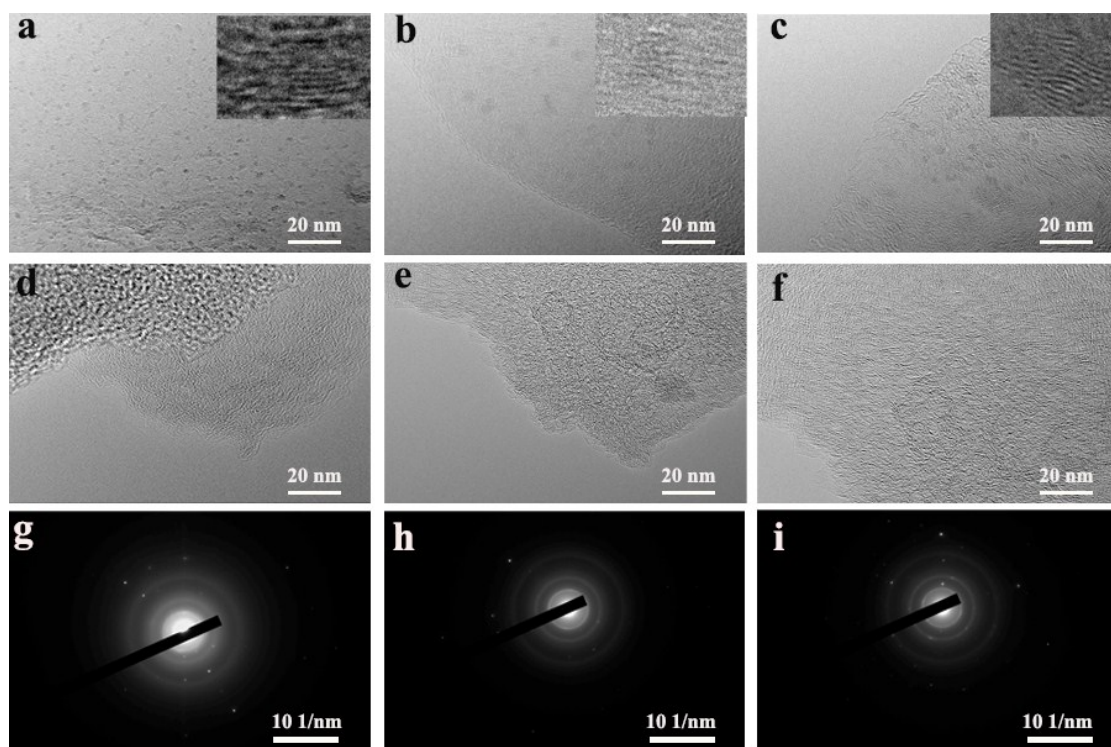


Figure S8. (a-f) HRTEM and (g-i) SAED images of **InFeCo@CNS900**. Top-right inset in a-c): enlarged HRTEM images of another selected Fe₄C nanoparticle displaying clear lattice fringe.

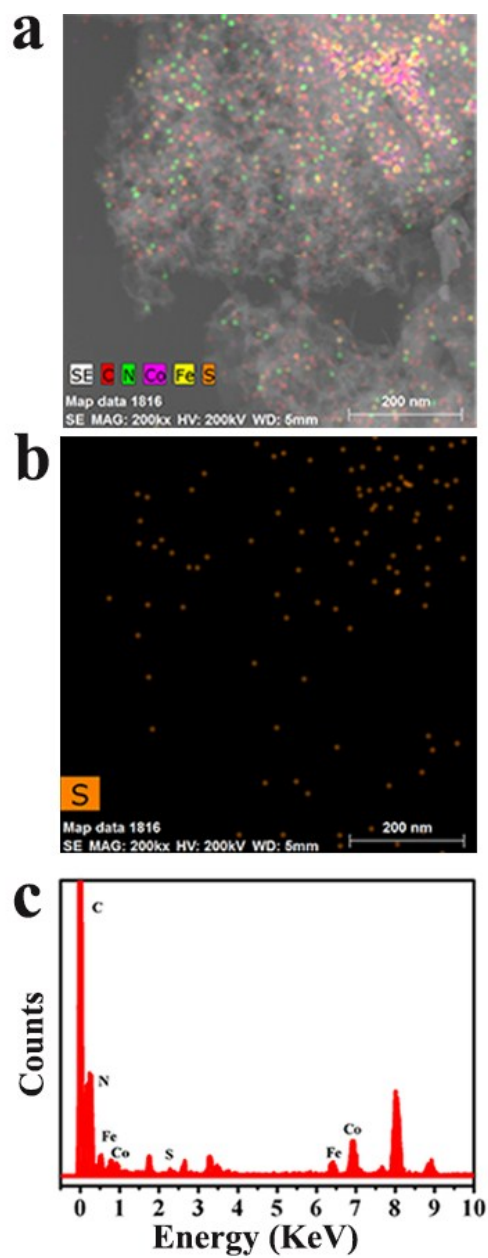


Figure S9. (a) Overlapped mapping of **InFeCo@CNS900**, (b) the mapping of S element and (c) EDS pattern of **InFeCo@CNS900**.

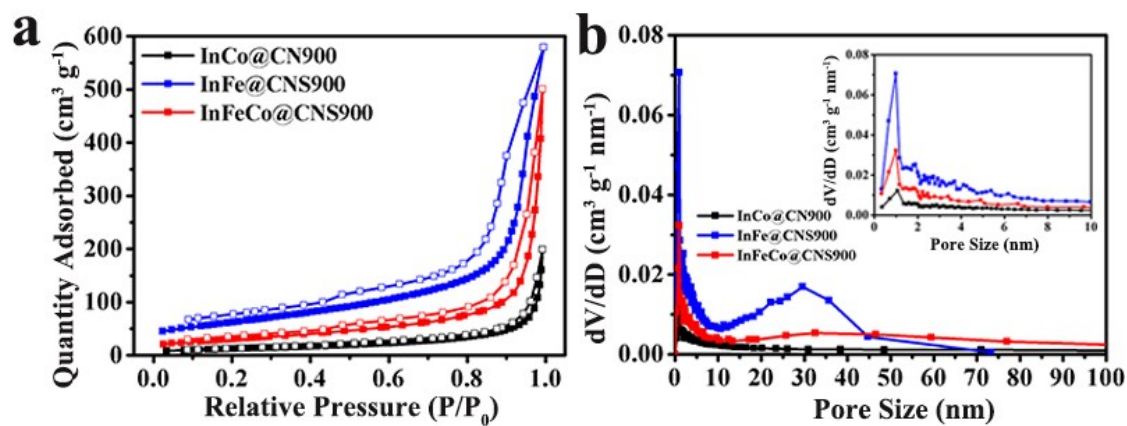


Figure S10. (a) N₂ isotherms at 77 K and (b) the corresponding NLDFT pore size distributions of InCo@CN900, InFe@CNS900, and InFeCo@CNS900.

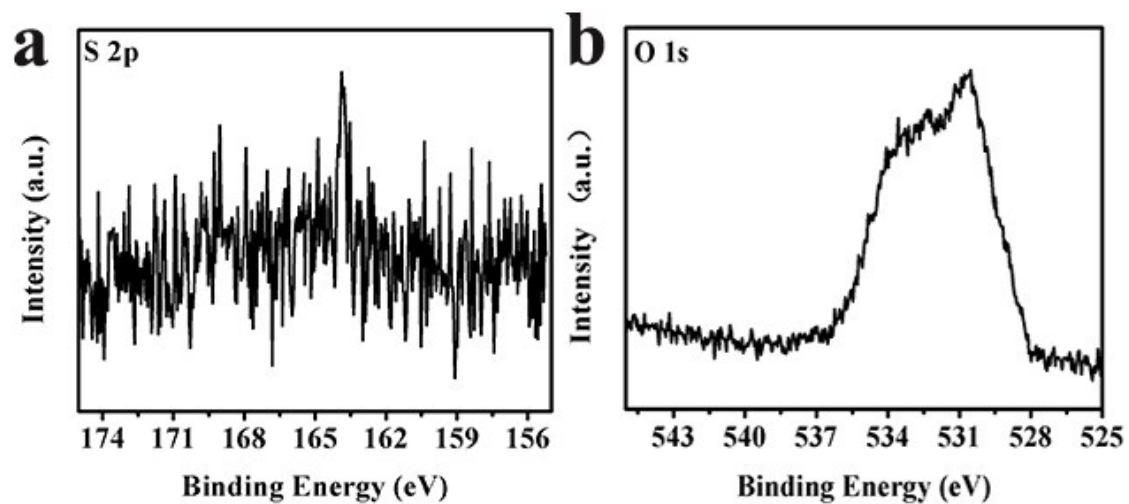


Figure S11. High-resolution (a) S 2p and (b) O 1s XPS spectra of **InFeCo@CNS900**.

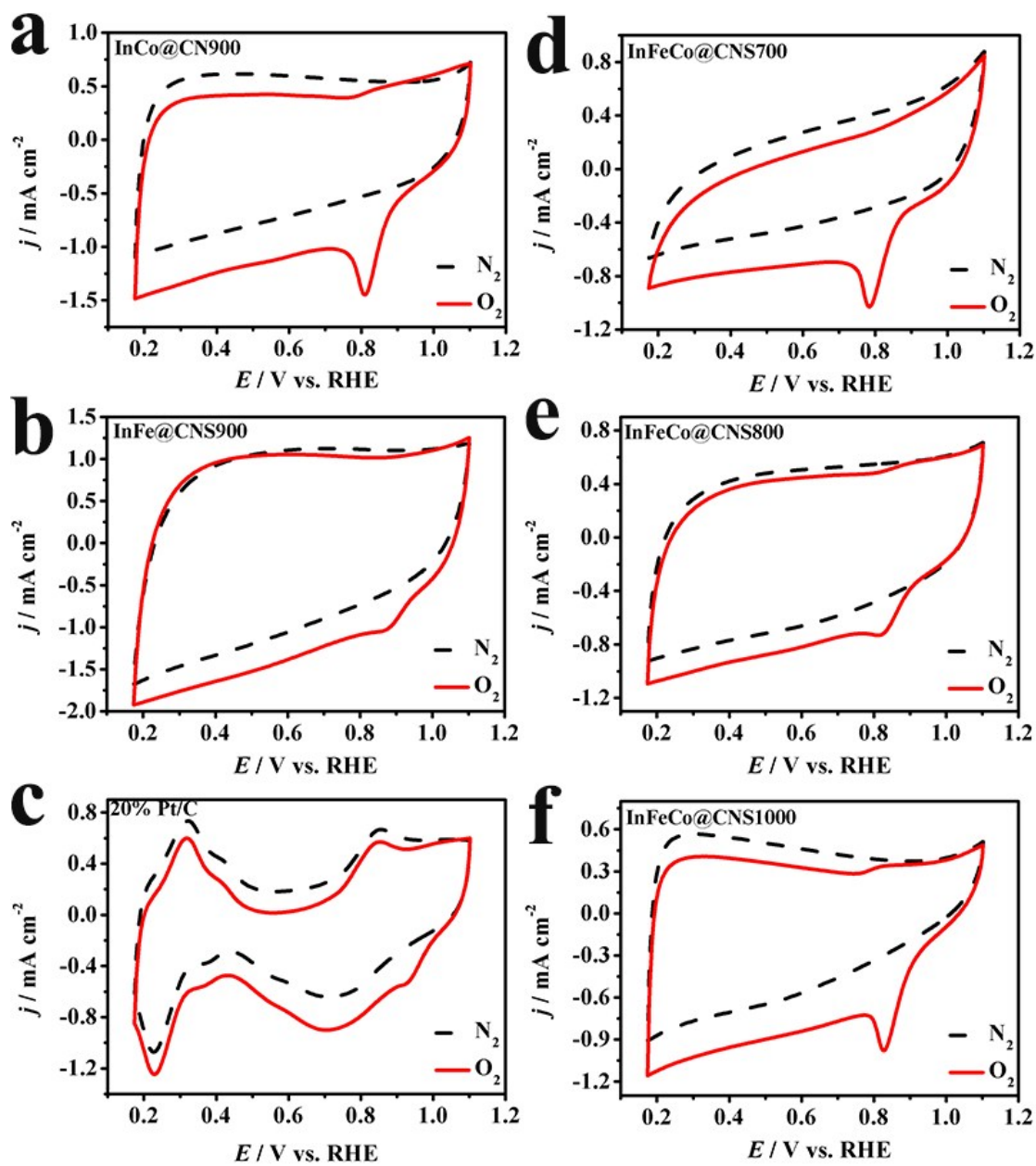


Figure S12. CV curves of (a) **InCo@CN900**, (b) **InFe@CNS900**, (c) **Pt/C** catalyst (d) **InFeCo@CNS700**, (e) **InFeCo@CNS800**, and (f) **InFeCo@CNS1000** in N_2 -/ O_2 -saturated 0.1 M KOH at $10 \text{ mV}\cdot\text{s}^{-1}$.

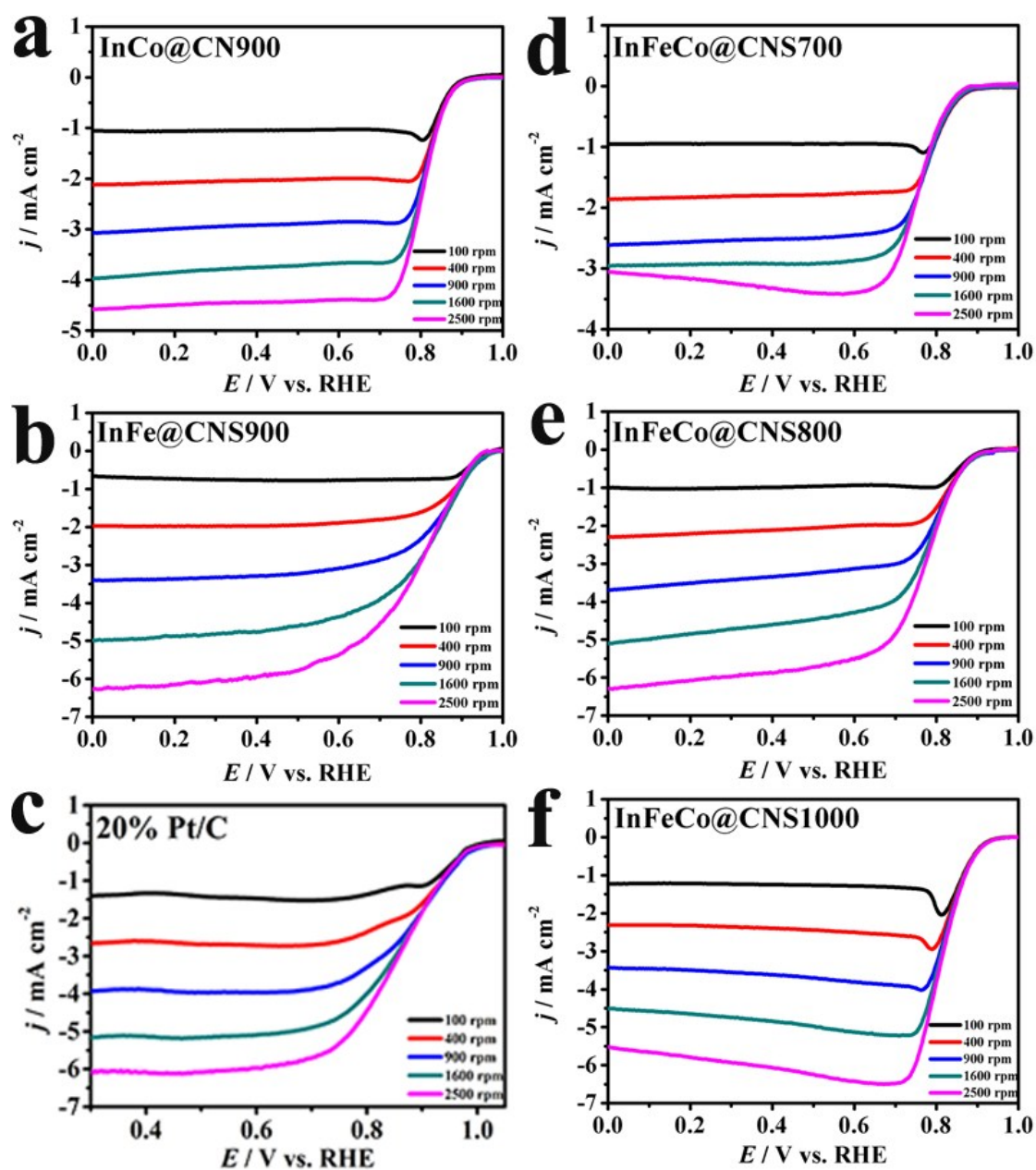


Figure S13. LSV curves at various rotating speeds of (a) **InCo@CN900**, (b) **InFe@CNS900**, (c) Pt/C catalyst (d) **InFeCo@CNS700**, (e) **InFeCo@CNS800**, and (f) **InFeCo@CNS1000**.

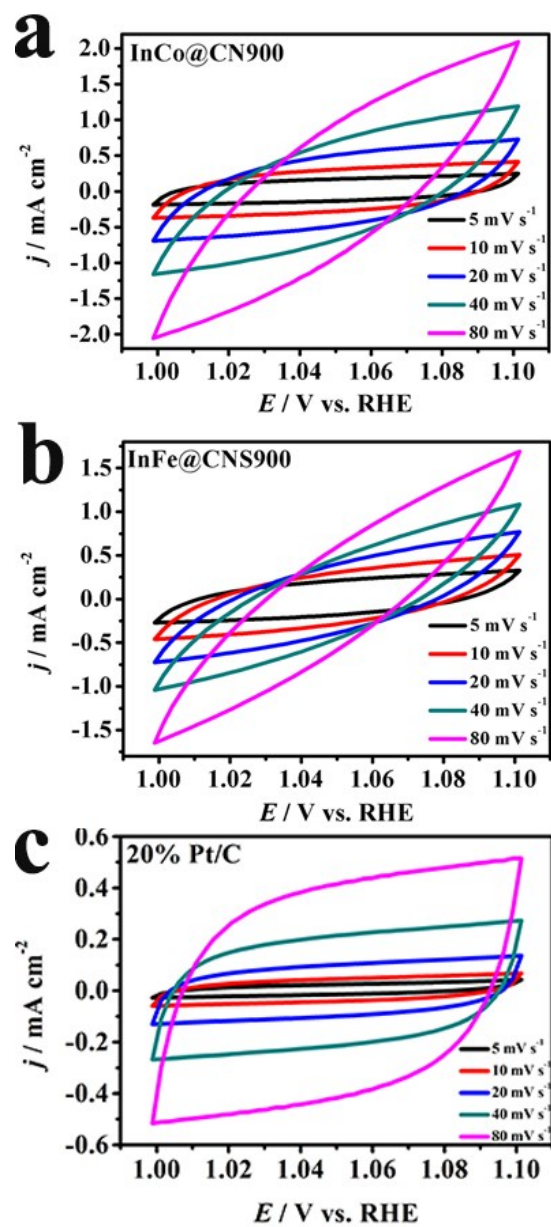


Figure S14. CV curves at different sweep speeds of (a) **InCo@CN900**, (b) **InFe@CNS900**, and (c) Pt/C catalyst.

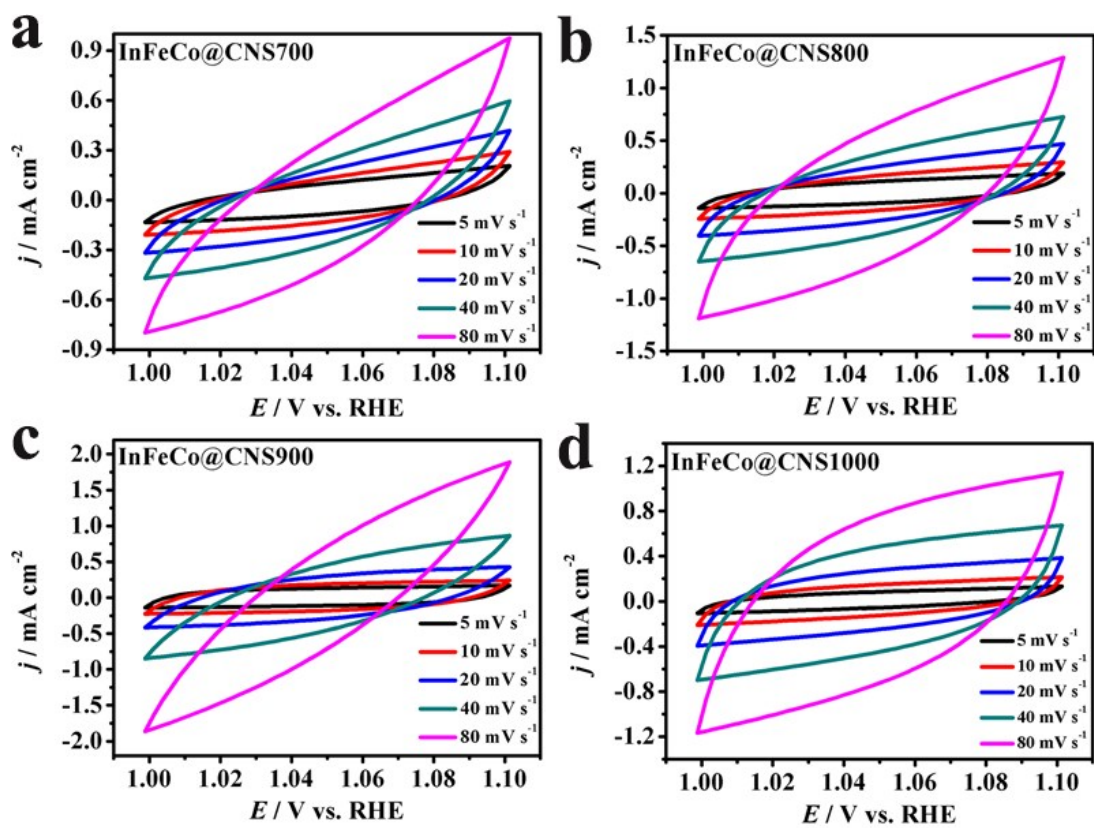


Figure S15. CV curves at different sweep speeds of (a-d) **InFeCo@CNS700-1000**.

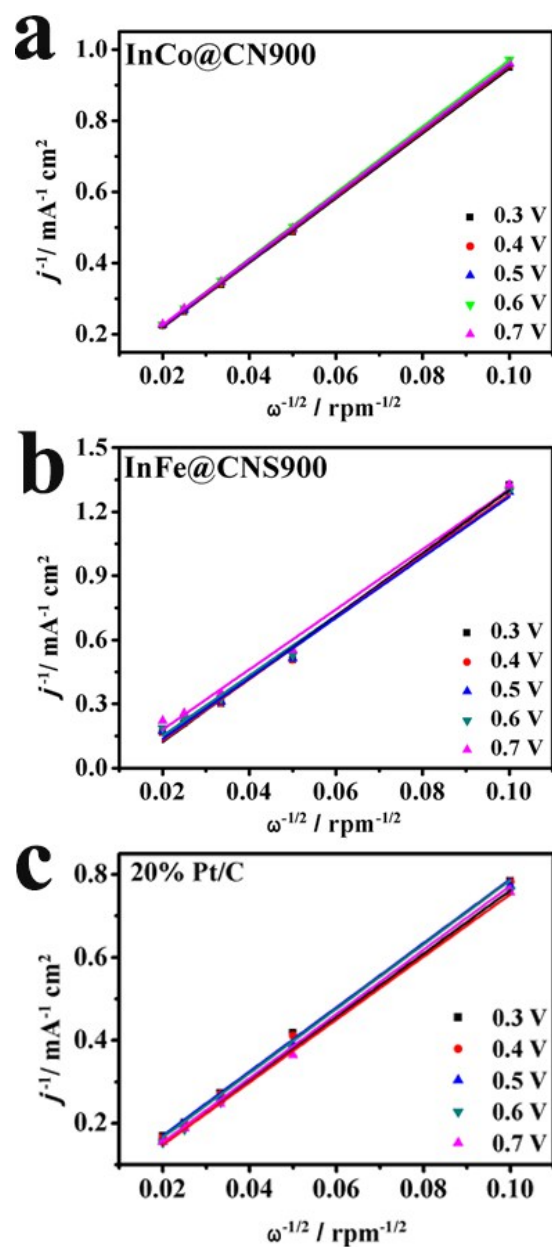


Figure S16. The K–L plots at various potentials of (a) **InCo@CN900**, (b) **InFe@CNS900**, and (c) Pt/C catalyst.

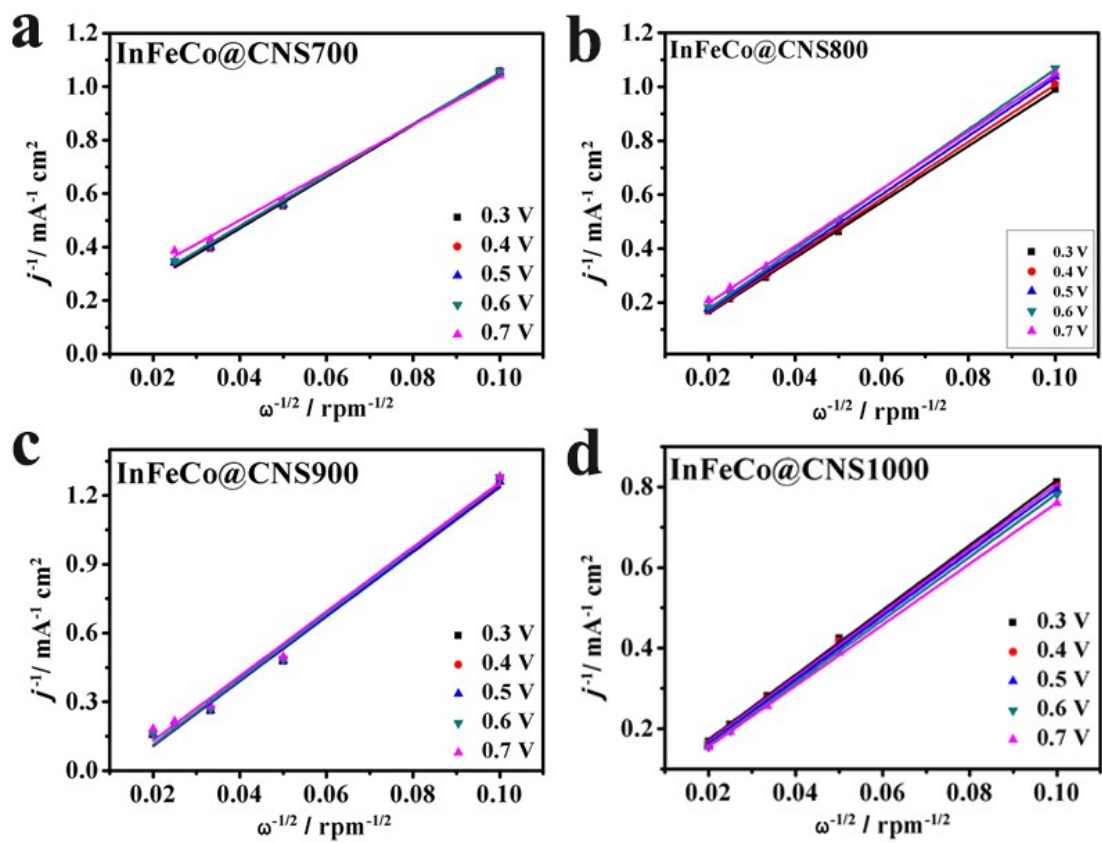


Figure S17. The K–L plots at various potentials of (a-d) InFeCo@CNS700-1000.

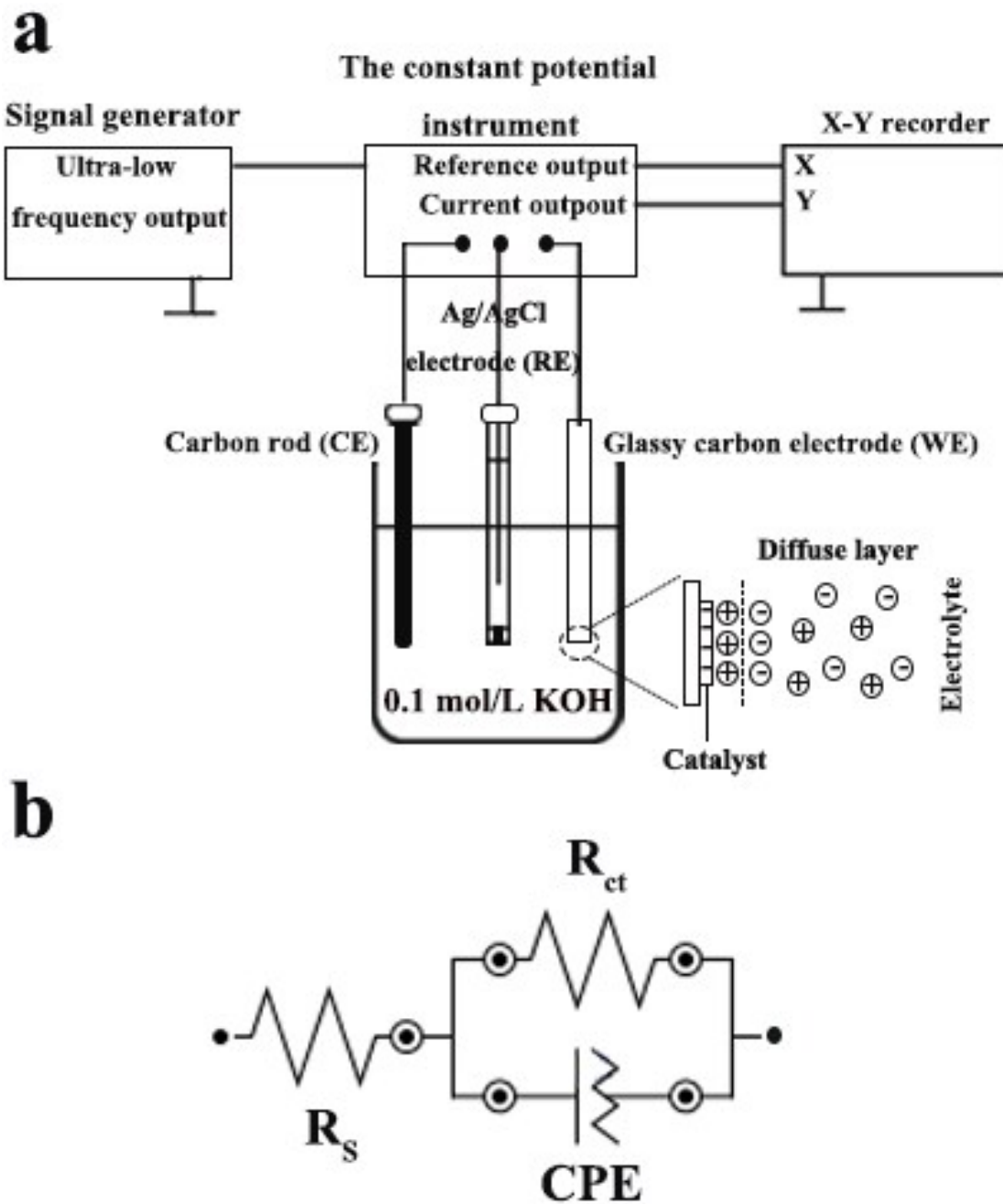


Figure S18. The experimental circuit (a) and the parallel analog circuit (b) of electrolytic cell.

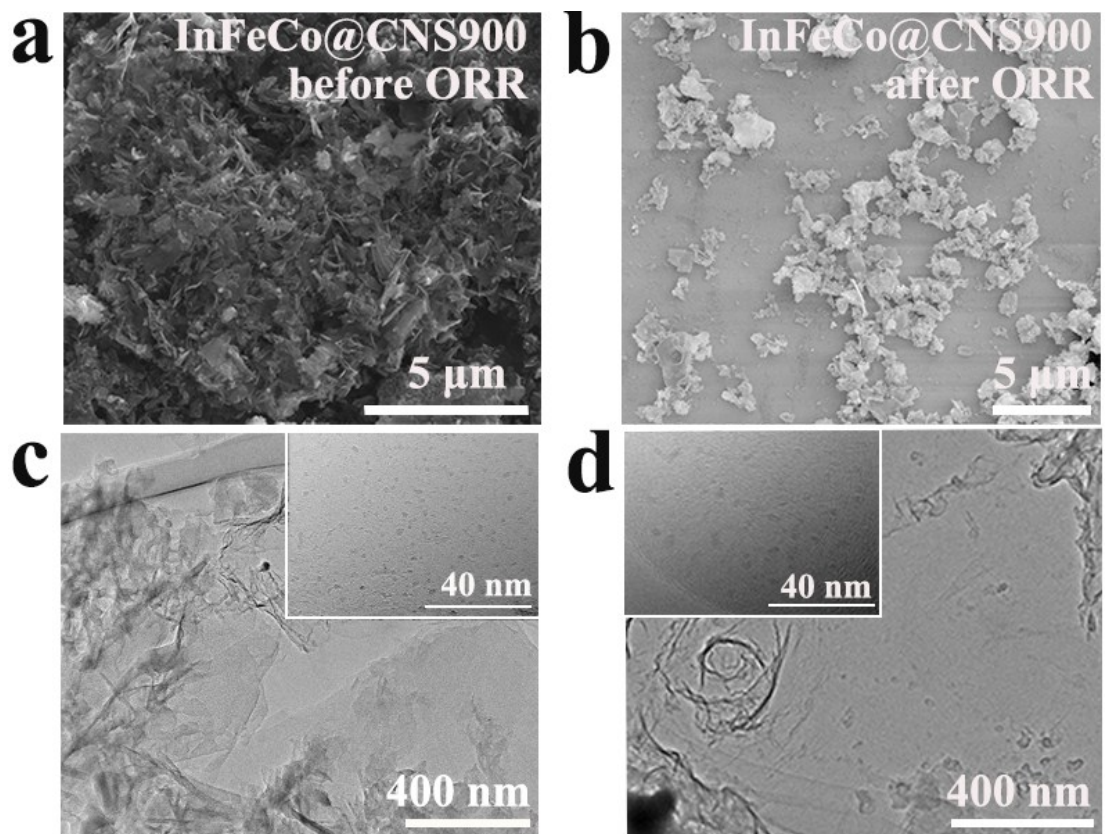


Figure S19. The SEM, TEM, and HRTEM patterns of (a, c) InFeCo@CNS900 before ORR and (b, d) InFeCo@CNS900 after ORR.

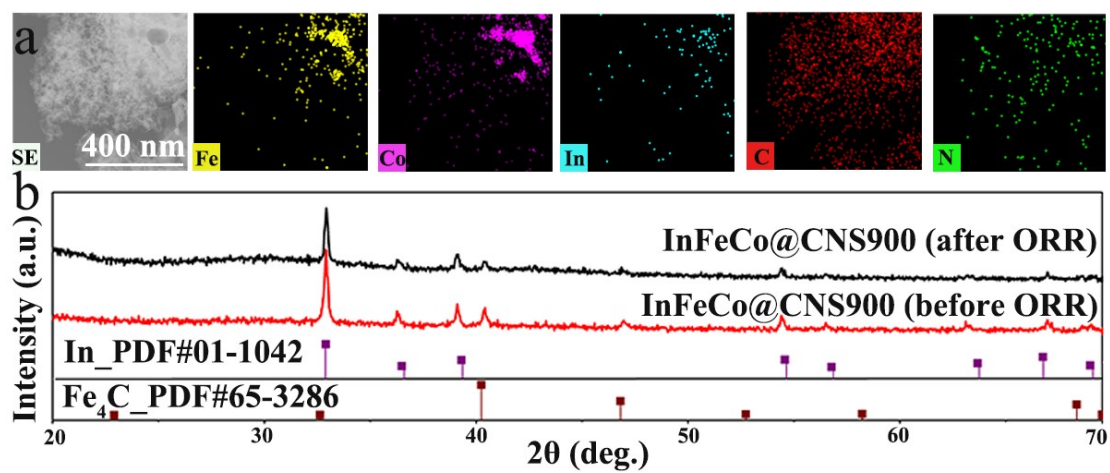


Figure S20. (a) The element mapping and (b) PXRD images of the **InFeCo@CNS900** after ORR.

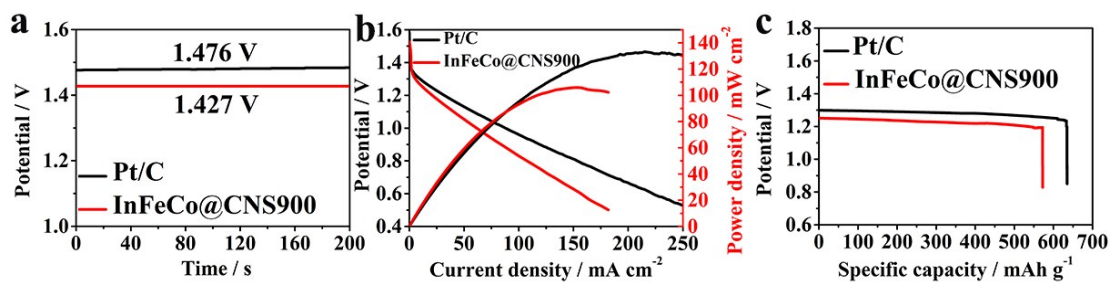


Figure 21. (a) Open-circuit voltage curves, (b) polarization and power density curves, and (c) galvanostatic discharge curves at 10 mA cm^{-2} of the **InFeCo@CNS900** and Pt/C based Zn-air batteries.

Table S2. Pore characteristics of all prepared materials.

Sample	Surface area /m ² ·g ⁻¹		Total pore volume ^a	Micropore volume ^a
	BET	Langmuir	/ cm ³ ·g ⁻¹	/ cm ³ ·g ⁻¹
InOF-24	434.13	819.28	0.3229	0.3036
Fe(SCN)₆@InOF-24	19.67	80.01	0.4228	0.0131
InCo@CN900	45.59	78.24	0.2842	0.0183
InFe@CNS900	219.83	351.56	0.7525	0.0943
InFeCo@CNS700	78.76	134.70	0.3904	0.0300
InFeCo@CNS800	79.88	139.81	0.4931	0.0315
InFeCo@CNS900	109.96	173.58	0.6298	0.0456
InFeCo@CNS1000	149.78	255.05	0.6992	0.0597

^a Determined by NLDFT method.

Table S3. C, N content measured from elemental analysis and N dopant proportions of **InFeCo@CNS900** catalysts measured from fitting of the N 1s XPS.

Sample	C /wt%	N /wt%	Relative content of different N species / 100%				$\frac{N_{(\text{pyridinic+graphitic})}}{N_{\text{total}}}/\%$
			pyridinic-N	pyrrolic-N	graphitic-N	oxidized-N	
InFeCo@CNS900	91.27	5.63	0.41	0.23	0.24	0.12	0.65

Table S4. Comparison of the non-noble metal catalysts with high ORR activity in 0.1 M KOH solution reported in kinds of literatures.

Catalyst ^a	E_{onset} (V)	$E_{1/2}$ (V)	n	$ J_L ^b$ (mA·cm ⁻²)	Reference
(Fe,Co)/CNT	1.15	0.954	/	/	[1]
Co-Fe/NC-700	/	0.854	3.81	/	[2]
Co-N@HCS	0.964	0.86	3.98	/	[3]
Co,N-CNF	0.882	0.809	/	5.71	[4]
Fe-N-DSC	1.025	0.833	4	/	[5]
NCNT-24-800	0.882	0.809	3.89-3.98	/	[6]
NCNF2-900	0.95	0.84	3.9-4.0	/	[7]
InCo@CN900	0.902	0.814	3.46	3.80	This work
InFe@CNS900	0.962	0.836	3.95	4.82	This work
InFeCo@CNS700	0.865	0.773	3.96	2.92	This work
InFeCo@CNS800	0.916	0.801	3.48	4.72	This work
InFeCo@CNS900	0.926	0.807	3.84	5.15	This work
InFeCo@CNS1000	0.928	0.823	3.61	4.75	This work

^a The samples listed in the table are the most efficient one chosen out from those reported in the corresponding literature, respectively.

^b The limited current densities (J_L) are compared at a rotation speed of 1600 rpm unless otherwise stated.

Table S5. Comparison of the carbon materials with Tafel slope, C_{dl} , ECSA and EIS in 0.1 M KOH solution.

Catalyst	Tafel slope ($mV \cdot dec^{-1}$)	C_{dl} ($mF \cdot cm^{-2}$)	ECSA ($m^2 \cdot g^{-1}$)	R_S (Ω)	R_{ct} (Ω)	CPE
InCo@CN900	57.6	9.86	24.65	26.29	19.09	0.83
InFe@CNS900	97.1	4.68	11.70	26.18	21.91	0.82
InFeCo@CNS700	66.6	3.69	9.23	29.27	53.25	0.86
InFeCo@CNS800	76.6	7.08	17.70	26.04	20.76	0.83
InFeCo@CNS900	59.5	8.82	22.05	26.18	19.03	0.85
InFeCo@CNS1000	46.9	8.95	22.38	21.61	18.31	0.86
20 wt% Pt/C	65.3	5.33	13.33	27.35	17.32	0.85

References:

- 1 J. Wang, W. Liu, G. Luo, Z. Li, C. Zhao, H. Zhang, M. Zhu, Q. Xu, X. Wang, C. Zhao, Y. Qu, Z. Yang, T. Yao, Y. Li, Y. Lin, Y. Wu, Y. Li, *Energy Environ. Sci.*, 2018, **11**, 3375-3379.
- 2 S. L. Zhang, B.Y. Guan, X. W. Lou, *Small*, 2019, **15**, 1805324.
- 3 S. Cai, Z. Meng, H. Tang, Y. Wang, P. Tsiakaras, *Appl. Catal. B: Environ.*, 2017, **217**, 477-484.
- 4 L. Shang, H. J. Yu, X. Huang, T. Bian, R. Shi, Y. F. Zhao, G. I. N. Waterhouse, L. Z. Wu, C. H. Tung, T. R. Zhang, *Adv. Mater.*, 2016, **28**, 1668-1674.
- 5 Z. Huang, H. Y. Pan, W. J. Yang, H. H. Zhou, N. Gao, C. P. Fu, S. C. Li, H. X. Li, Y. F. Kuang, *ACS Nano*, 2018, **12**, 208-216.
- 6 P. C. Shi, J. D. Yi, T. T. Liu, L. Li, L. J. Zhang, C. F. Sun, Y. B. Wang, Y. B. Huang, R. Cao, *J. Mater. Chem. A*, 2017, **5**, 12322-12329.
- 7 D. Guo, H. Wei, X. Chen, M. Liu, F. Ding, Z. Yang, Y. Yang, K. Yang, S. Huang, *J. Mater. Chem. A*, 2017, **5**, 18193-18206.